Decoherence Cross-Section in NO + Ar Collisions: Experimental Results and a Simple Model

ARTICLE *in* THE JOURNAL OF PHYSICAL CHEMISTRY A · APRIL 2013

Impact Factor: 2.69 · DOI: 10.1021/jp401005v · Source: PubMed

5 AUTHORS, INCLUDING:

Jesus Tornero

Complutense University of Madrid

9 PUBLICATIONS **73** CITATIONS

SEE PROFILE

Steven Stolte

Jilin University

236 PUBLICATIONS **4,128** CITATIONS

SEE PROFILE

A. González Ureña

Complutense University of Madrid

282 PUBLICATIONS **1,605** CITATIONS

SEE PROFILE

THE JOURNAL OF PHYSICAL CHEMISTRY A

Article

pubs.acs.org/JPCA

Decoherence Cross-Section in NO + Ar Collisions: Experimental Results and a Simple Model

M.-S. Chao,[‡,§,▽] J. Tornero,[†,▽] K. C. Lin,[‡,§] S. Stolte,[∥,⊥,#] and A. González Ureña*[,†]

[†]Unidad de Láseres y Haces Moleculares Instituto Pluridisciplinar, Universidad Complutense de Madrid; Madrid-28040, Spain

[‡]Department of Chemistry, National Taiwan University, Taipei 106, Taiwan

[§]Institute of Atomic and Molecular Sciences, Academia Sinica, Taipei 106, Taiwan

[∥]Institute of Atomic and Molecular Physics, Changchun, 130012, China

[⊥]Laser Center and Department of Physical Chemistry, Vrije Universiteit, Amsterdam, De Boelelaan 1083, 1081 HV Amsterdam, The Netherlands

[#]Laboratoire Francis Perrin, Bâtiment 522, DRECEM/SPAM/CEA Saclay, 91191 Gif sur Yvette, France

ABSTRACT: Quantum decoherence can be viewed as the mechanism responsible for the quantum-to-classical transition as the initially prepared quantum state interacts with its environment in an irreversible manner. One of the most common mechanisms responsible for the macroscopically observed decoherence involves collisions of an atom or molecule, initially prepared in a coherent superposition of states, with gas particles. In this work, a coherent superposition of quantum internal states of NO molecules is prepared by the interaction between the molecule with both a static and a radiofrequency electric field. Subsequently, NO + Ar collision decoherence experiments are investigated by measuring the loss of coherence as a function of the number of collisions. Data analysis using a model based on the interaction potential of the collisional partners allowed to unravel the molecular mechanism responsible for the loss of coherence in the prepared NO quantum superposition of internal states. The relevance of the present work relies on several aspects. On the one hand, the use of radio-waves introduces a new way for the production of coherent beams. On the other hand, the employed methodology could be useful in investigating the Stereodynamics of chemical reactions with coherent reagents.

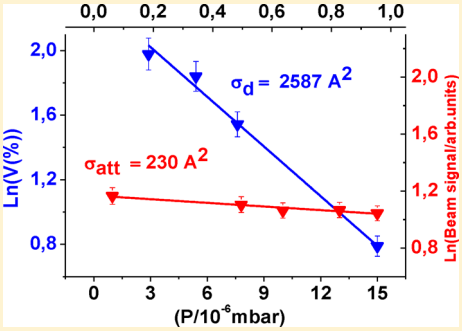

INTRODUCTION

The coherence between quantum internal states of atoms and molecules is nowadays exploited in various applications as quantum computing,[1] Ramsey interferometry,[2] coherent control in molecular dynamics,[3,4] or stereochemistry[5] to cite just a few examples.

In the quantum mechanical world, the loss of coherence or the "non-random" relation of the phase angles between the components of a system in a quantum superposition, the so-called quantum decoherence, constitutes a subject of increased interest and research since the late 20th Century.[6,7]

Decoherence is therefore viewed as the mechanism underlying the onset of the classical limit from an initial quantum state as the system's interaction with its environment takes place in an irreversible manner. As a result, experiments based on monitoring the progressive decoherence of an initially prepared superposition of states[8,9] are implemented in order to investigate the quantum-to-classical transition,[10−14] a subject still under debate.

One of the most natural and accepted mechanisms responsible for the macroscopically observed decoherence involves the presence of collisions with gas particles. Indeed collisions with gas molecules localize the center-of-mass wave function causing a reduced visibility of the interference pattern.

Most of the collision decoherence experiments published in the literature implied the loss of coherence of the prepared atom or molecule in a quantum superposition of external states. For example, collisional decoherence has been observed in matter-wave interferometry using massive C70-fullerene molecules inside a Talbot−Lau interferometer.[14]

In the present work we first show how the interaction between an oscillating radio frequency (RF) field and a static DC field with a beam of NO molecules produces a coherent beam whose manifestation is the onset of interferences in the forward beam intensity.[15]

After the formation of a NO coherent beam, collisions with Argon are produced under beam-gas conditions and the loss of coherence is monitored by measuring the visibility reduction as a function of the Argon scattering pressure. Afterward, both the total scattering and the decoherence collision cross section are deduced from the experimental data and compared with relevant theoretical models. We will show that the dynamics

Special Issue: Stereodynamics Symposium

Received: January 29, 2013
Revised: March 14, 2013
Published: April 5, 2013

   dx.doi.org/10.1021/jp401005v | J. Phys. Chem. A 2013, 117, 8119−8125

underlying the total scattering and the decoherence of the NO beam imply a different collision mechanism.

The originality and relevance of the present work rely on several aspects. On the one hand, the use of radio-waves introduces a new way for the production of coherent beams and for manipulating polar molecules. On the other hand, the present methodology, when satisfactorily applied to more collision systems could be useful to investigate quantum decoherence and, perhaps, in designing quantum computing experiments. Finally, to cite just one more application example, the present methodology could be used in investigating the stereodynamics of chemical reactions with coherently prepared reagents.

EXPERIMENTAL SETUP

The main details of the experimental technique have been described elsewhere.[15] Thus, only a brief summary is described here for a better understanding of the experimental results.

As it is illustrated in Figure 1, from the experimental point of view and with respect to ref 15, the more important change made was the use of the RF chamber as the scattering chamber as well. In this figure, both side and top views of the molecular beam apparatus are shown. In addition, Table 1 lists the more relevant experimental parameters in order to understand the present investigation and conclusions.

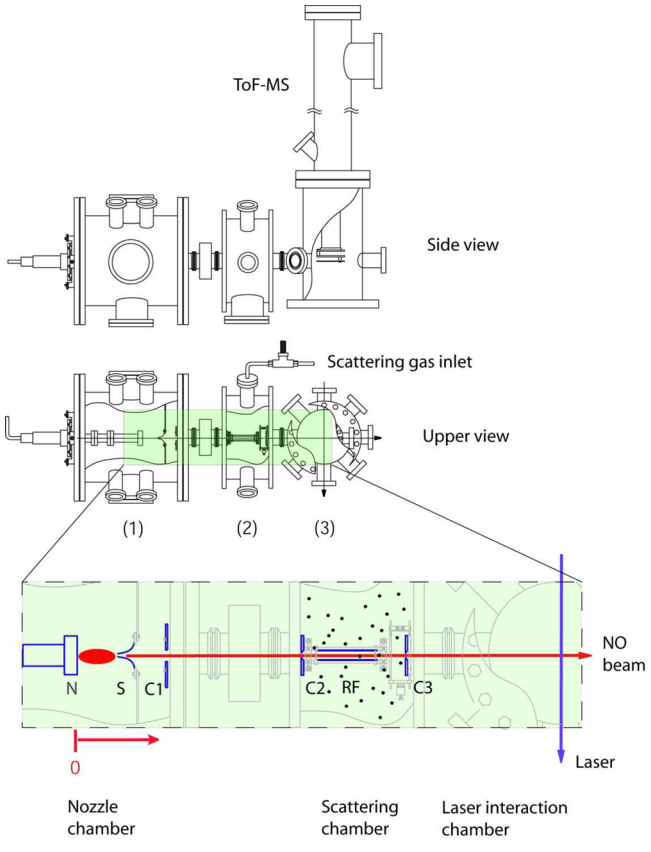

Figure 1. Schematic side and upper view of the molecular beam apparatus. The beam divergence is about 1.5 mrad. The total length of the scattering chamber is about 164 mm. The experimental setup consists of three main chambers: the nozzle chamber including the nozzle (N), the skimmer (S) and the first aperture (C_1), the scattering chamber where the radio frequency unit (RF) is allocated between two apertures (C_2 and C_3), and the laser interaction chamber where the NO ions are generated. Further experimental details can be found in Table 1 and ref 15.

Table 1. Relevant Experimental Conditions

NO Beam	
nozzle oven temperature (K)	300−320
peak velocity, v_{mp} (ms^{-1}) /10^3	1.1
full-width half-maximum (%)	10
beam divergence (deg)	0.7
nozzle-detector distance (m)	6.5×10^{-1}
stagnation pressure (bar)	2−4
Scattering Chamber	
Ar pressure (10^{-6} mbar)	0−15
length (m)	1.6×10^{-1}
temperature (K)	298
Resonant Unit (Stark and RF Field)	
length (m)	$8 \cdot 10^{-2}$
width (m)	$6.7 \cdot 10^{-3}$
DC field, E ($kV \cdot m^{-1}$)	11.94
RF field amplitude, E_1 ($kV \cdot m^{-1}$)	3.1
frequency range (kHz)	1400−1450

As the polar molecule travels inside the RF unit, the basic interactions that take place correspond to those of the molecule with a static DC field and with an oscillating RF field. Whereas the homogeneous field produces Stark splitting for a given J, the RF field is tuned to produce a coherent superposition between the Stark levels. Because the RF field originates a distinct interaction potential with each of the coupled Stark levels, a phase shift is introduced between them leading to interferences, manifested in oscillations of the total beam intensity when it is measured as a function of the RF frequency (see ref 15 for further details).

There is no doubt that by introducing a scattering gas, Ar in the present investigation, the total beam intensity will be attenuated. However, our motivation was to investigate whether, in addition to the loss of beam intensity, there is also a loss of coherence and, if so, to monitor it as a function of the scattering gas pressure. This was, therefore, the motivation to introduce the scattering gas right at the same location where the coherent NO beam was produced.

Essentially, the main steps of the experiment consisted of (i) the production of a supersonic beam of NO (20%) diluted in helium (80%) (nozzle chamber in Figure 1), (ii) the interaction of the polar NO molecule with a static and a RF (scattering chamber in Figure 1) field, and, finally, (iii) the monitoring of both the beam intensity and the interferences visibility as a function of the number of collisions between the NO and Ar, as the pressure of the rare gas is changed in the scattering cell.

At the experimental conditions of both DC and RF electric fields employed in this investigation, the main induced NO transition moment corresponds to the $J = \Omega = 3/2$; $\Delta M = \pm 1$ transition.[15] As in previous works, the NO beam intensity was monitored by UV-laser ionization (see the laser interaction chamber in Figure 1 and ref 15).

SIMPLE WAVE MODEL

In this section, a brief summary of the *two level interaction* model described in ref 15 is presented for a better understanding of the results.

dx.doi.org/10.1021/jp401005v | J. Phys. Chem. A 2013, 117, 8119−8125

The interaction of such a model with an electromagnetic field $\varepsilon = E_1 \cos \omega t$ under an electric-dipole approximation is a well-known case whose Hamiltonian can be written as

$$H = H_o - \mu_{ab} E_1 \cos \omega t = H_o - \mu_{ab} \frac{E_1}{2} (e^{i\omega t} + e^{-i\omega t}) \quad (1)$$

where μ_{ab} is the dipole moment of the $a \rightarrow b$ transition, ω is the angular frequency of the oscillating field, and H_o is the unperturbed Hamiltonian. The non-degenerate two-level system is characterized by the time-dependent wave function $\Psi(t)$ given by

$$\Psi(t) = a(t) e^{-i\omega_a t} \phi_a + b(t) e^{-iw_b t} \phi_b \quad (2)$$

where $a(t)$ and $b(t)$ are the coefficients of the lower and higher states ϕ_a and ϕ_b, respectively. Their expressions using the rotating wave approximation (RWA) are given in ref 15. Here the energies of the two states are $E_a = \hbar\omega_a$ and $E_b = \hbar\omega_b$ so that the energy difference $\omega_o = \omega_b - \omega_a$ is the resonant angular frequency, i.e., $\omega_0 = 2\pi\nu_0$.

When the oscillating ε field is applied, the time evolution of the molecular state (and thus that of the electric dipole moment) is governed by the generalized Rabi frequency Ω', which is given by[15]

$$\Omega' = \sqrt{\Lambda^2 + \Omega_R^2} \quad (3)$$

where $\Lambda = \omega - \omega_o$ and Ω_R is given by

$$\hbar\Omega_R = \mu_{ab} \cdot E_1 \quad (4)$$

It can be shown[15] that under our experimental conditions the beam signal can be expressed as

$$S \approx C(1 + \langle u_2 \rangle) \quad (5)$$

where C is a constant that depends on the particle density and other experimental factors[15] and $\langle u_2 \rangle$ stands for the velocity average value of u_2 given by

$$u_2 = \left(p^2 - \frac{\Lambda^2}{\Omega'^2} q^2 \right) \cos(\Lambda t + \varphi_{ab}) + \frac{2\Lambda}{\Omega'} pq \sin(\Lambda t + \varphi_{ab}) + \frac{\Omega_R^2}{\Omega'^2} q^2 \cos(\Lambda t - \varphi_{ab}) \quad (6)$$

In our experiment, the perturbation associated to dipole molecule interaction with the RF field is equal to or less than a few megahertz, i.e., equal or less than 10^{-9} eV. This energy is far less than the molecule kinetic energy, in our case on the order of 0.1 eV. Thus, the only action of the potential reduces to an action on the internal component part of the wave function. In this view, the phase shift can be estimated using only the interaction potential between the induced dipole and the RF field. The result is given by[15]

$$\Delta\varphi_{ab} = t \left[\cdot \frac{\Omega_R^2}{\Omega'} \sin \Omega' t \cdot \sin 2\omega t - \frac{4\Omega_R^2 \cdot \Lambda}{\Omega'^2} \cdot \sin^2 \frac{\Omega' t}{2} \cdot \cos^2 \omega t \right] \quad (7)$$

It should then be remarked that, contrary to other scenarios[10] in which interference measurements in the beam intensities refer to translational degrees of freedom and are performed in configuration space, in the present case, the degrees of freedom are internal, and visibilities are observed in the frequency domain.

As listed in Table 1 (see also ref 15), since the 1400−1450 kHz frequency range explored in the present investigation lies above the resonant frequency of ω_0 = 1200 kHz and is far greater than the estimated Rabi frequency of Ω_R = 27 kHz,[15] the approximation $\Lambda \gg \Omega_R$ seems to be appropriate to estimate the beam signal given by eqs 5−7. Under these conditions, one can show, after some algebra, that the beam intensity oscillates according to

$$S \sim 1 + \cos(\Omega_R t/\Lambda) \quad (8)$$

Equation 8 clearly indicates that even far from resonant conditions, the forward beam intensity will show oscillations as long as the RF field is on (i.e., providing Ω_R is not null).

At present, we are developing a new full theoretical treatment of the molecule field interaction based on *the dressed state picture*, which presents the molecular beam intensity oscillations in a more clear and natural manner. This study will be the subject of a forthcoming paper.

RESULTS AND DISCUSSION

Figure 2 displays the NO beam intensity measured as a function of the RF field frequency over the 1400−1450 kHz range for two distinct Ar scattering pressures, as indicated. In both cases the beam signal oscillations as the RF frequency is changed are clearly manifested. A closer look at the data indicates that the visibility, V, of the oscillation, defined by

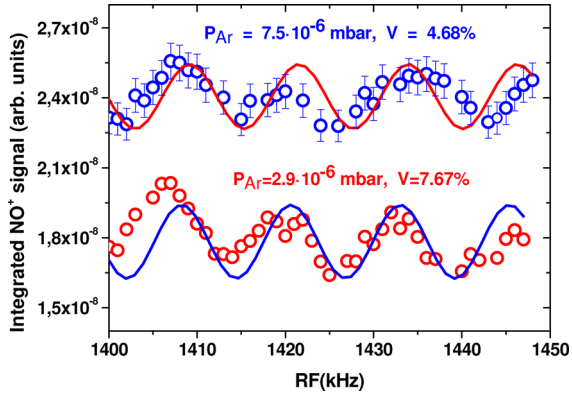

Figure 2. Transmitted beam signal as a function of the RF field frequency at distinct Ar scattering pressures as indicated. While maintaining the visibility and for the sake of clarity, the average signal of top panel data has been shifted upward. Notice the similarity in the oscillations. The solid red and blue lines are the best fits to the experimental data (open circles). Except for the different fringes' visibility, both fits show the same phase and frequency oscillation. Estimated error bars (4%) are shown in the top part. Similar errors (not shown) were estimated in runs taken at different scattering pressures.

$$V = (S_{max} - S_{min})/(S_{max} + S_{min}) \quad (9)$$

where S_{max} and S_{min} stand for the maximum and minimum beam signal, respectively, decreases as the Argon pressure increases. This trend is also confirmed at other scattering pressures not shown in Figure 2.

A comparison between two spectra of different visibilities is depicted in Figure 3 .For the sake of clarity they have been normalized to the same average signal. Notice that despite their

dx.doi.org/10.1021/jp401005v | J. Phys. Chem. A 2013, 117, 8119−8125

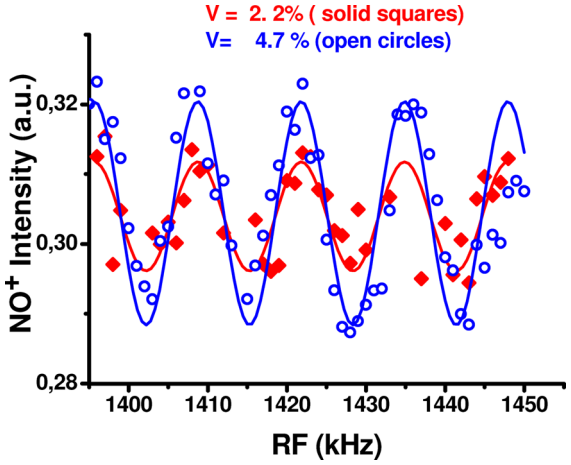

Figure 3. Comparison between two spectra of different visibilities, as indicated. They correspond to the following scattering pressures: lower (higher) visibility 15×10^{-6} (7.5×10^{-6}) mbar. For the sake of clarity, they have been normalized to the same average signal. Notice that despite their different intensities, the oscillations show the same frequency and phase. See text for comments.

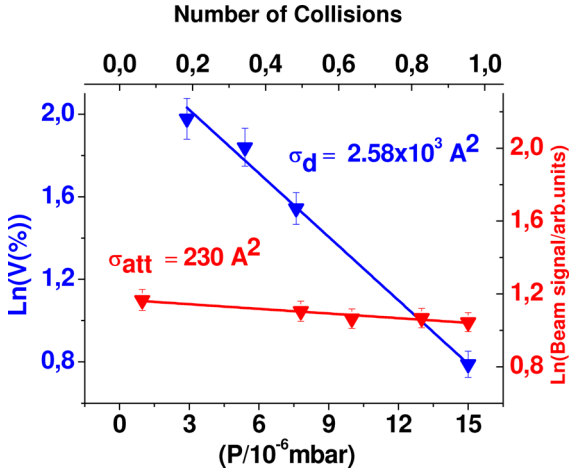

Figure 4. Blue triangles: Lambert−Beer type of representation for the NO beam attenuation induced by Ar scattering. Red triangles: same type of representation but for the loss of visibility. Solid lines: the respective best fits using eq 10 of the text, from where the corresponding cross sections were deduced. Notice the ca. 1 order of magnitude difference between both cross sections. The bottom *x*-axis is the Ar scattering pressure. The top *x*-axis corresponds to the he total number of NO+ Ar collisions occurred after the NO passed through the scattering chamber. The bars represent an estimated error of 4%. See text for comments.

different intensities, the oscillations show the same frequency and phase. In other words, neither the frequency of the oscillation, estimated to be 12.2 kHz ± 0.3 kHz, nor its phase show dependence on the Ar scattering pressure.

Decoherence Cross-Section Model. Several theoretical models have been developed to relate the expected loss of interference to decoherence theory[10−14] using the so-called decoherence function, which describes the loss of coherence after one scattering event. One of the most used models is based on the strong coherence limit. In this situation, the spatial coherence of the center of mass state is large enough such that every collision leads to a complete loss of coherence. In this picture, the visibility is given as a function of the scattering pressure p by[10]

$$V(p) = V_0 \cdot \exp(-p/p_0) \tag{10}$$

where the loss of coherence with increasing pressure is described by p_0, the so-called "decoherence pressure", which is determined by the effective decoherence cross-section σ_d and l, the length of the scattering chamber by the relation

$$p_0 = kT/\sigma_d l \tag{11}$$

Here k is the Boltzmann constant, and T is the scattering gas absolute temperature. Replacing the value of p_0 in eq 10, one then obtains

$$V(N_g) = V_0 \cdot \exp(-N_g \sigma_d l) \tag{12}$$

where N_g denotes the scattering gas particle density.

In fact, eq 12 adopts the form of a Beer−Lambert type of equation describing the loss of coherence rather than the beam attenuation.

The semilog plot of the NO loss of beam intensity and loss of visibility induced by Ar scattering is depicted in Figure 4. Symbols represent experimental data. Solid lines show the respective best fits using the Beer−Lambert equation for the attenuation data and eq 10 below for the visibility data. The respective, cross-section values also indicated in the Figure, were deduced from the corresponding slopes. That the attenuation data can be well described by the Beer−Lambert functionality was the obvious expectation. However, the excellent fit of the loss of visibility by eq 10 was not that obvious and will be discussed further below.

The single collision condition character of the beam-gas experiment is manifested by the estimated number of bimolecular collisions taking place by the coherent NO molecule while crossing the Ar scattering chamber. As shown in the top *x*-axis of Figure 4, the whole set of data was taken for a number of collisions equal to or less than 1.

Probably one of the most remarkable, unexpected and interesting results of the present investigation is the great difference between both cross-section values. While the attenuation value is σ_{att} = 230 Å^2, that of decoherence amounts to $\sigma_d = 2.58 \times 10^3$ Å^2, i.e., approximately 1 order of magnitude higher. This significant difference could indicate the presence of a different mechanism responsible for quantum decoherence than for beam attenuation. This matter will be discussed below.

The validity of eq 10 to unambiguously describe the evolution of the effective decoherence cross-section as a function of the scattering pressure is well documented in the literature. As an example, the reader is referred to ref 10, specifically to Figures 2 and 3 of that publication.

The satisfactory fit of the visibility data shown in Figure 4 by eq 10 indicates that each collision leads to a complete loss of coherence. In principle, the effective cross-section value deduced from the semilogarithmic plot slope, $\sigma_d = 2.58 \times 10^3$ Å^2, was unexpectedly high. It was also surprising that it was almost 10 times higher than the total scattering cross-section value given by σ_{att} = 230 Å^2 as also deduced from the slope of the total attenuation plot of Figure 4 data.

Under our beam-gas experimental conditions, the reactants' relative velocity can be estimated[16] by

$$\bar{v}_R = \left(\frac{4}{\pi}\right)^{1/2} \sqrt{\frac{2E_\alpha}{\mu_{red}}} \tag{13}$$

dx.doi.org/10.1021/jp401005v | J. Phys. Chem. A 2013, 117, 8119−8125

where E_α is given by

$$E_\alpha = \frac{1}{2}\mu_{red}(v_g^2 + v^2{}_{NO}) \quad (14)$$

with μ_{red} being the system reduced mass, e.g.,

$$\mu_{red} = \frac{m_{Ar}\cdot m_{NO}}{m_{Ar} + m_{NO}} \quad (15)$$

Here v_g and v_{NO} are the most probable velocities of the scattering gas and NO beam, respectively. Thus, taking into account that the experimental peak NO velocity is $\sim 1.1 \times 10^3$ $m\cdot s^{-1}$, eq 13 gives an average relative velocity of $\overline{v}_R = 1.3 \times 10^3$ $m\cdot s^{-1}$ for an argon temperature of 298 K.

Fortunately, the NO + Ar total collision cross-section has been accurately measured over a wide range of relative velocity by Thuis et al.[18,19] From these measurements one obtains a collision cross-section value of 2.58×10^3 Å^2 at the same relative velocity, which compares well (within 10% of deviation) with our 230 Å^2 value.

The satisfactory agreement between the present and previously reported values of the attenuation cross-section for the NO + Ar system under study provides additional support to rule out any possibility of mere coincidence to justify the observed agreement.

Now arises the question of how to explain that the decoherence cross-section is about 1 order of magnitude higher than that of total attenuation.

In principle, one might argue that because the signal becomes weaker as the NO beam traverses the Ar scattering chamber, this could also lead to a decrease in the oscillations and therefore in their visibility. However, a closer inspection of the data, in particular of Figure 4, reveals that the loss of the beam intensity due to the argon scattering has a minor effect, if any, in the loss of beam coherence.

Indeed, looking at Figure 4 data over the high pressure range, one can note that an increase of the argon pressure from 13 to 15×10^{-6} mbar, that is, an increase of 15.4%, leads to a reduction of 24.7% in the beam visibility, while the beam intensity experiences a reduction of 1% only. In other words, over this range of scattering pressures, the oscillation visibilities changed significantly while the beam intensity hardly varied at all. Moreover, similar conclusions can be drawn by analyzing the evolution of these two pieces of data over the whole range of scattering pressures.

Clearly, only a different collision dynamics underlying these two phenomena, i.e., the total attenuation and the loss of coherence, can be responsible for the 1 order of magnitude difference between the two cross-section values.

For the total beam attenuation, it is obvious that the NO + Ar interaction potential scatters the NO out of the forward beam direction defined by the geometrical beam divergence ($\beta \leq 1.5$ mrad). Indeed, the loss of beam intensity as a function of the Ar pressure follows a Lambert−Beer dependence from which a σ_{att} can be extracted.

When the colliding NO molecule is prepared in a coherent superposition of states the loss of coherence, i.e., the loss of visibility, has little, if any, relation with the loss of forward beam intensity since the coherence can be lost while the NO molecules still travel along the forward beam direction.

As it was mentioned further above, the physical manifestation of the beam coherence is the presence of oscillations in the forward beam intensity as the RF field frequency is changed; oscillations which under the experimental conditions of our investigation show a frequency spacing of $\Delta\nu_{osc} = 12.2$ kHz. It therefore becomes clear that the loss of visibility must be necessarily due to an interaction between the NO whose dipole moment experiences this "coherent oscillation" and the incoming Ar atom.

In this view, not all relative configurations of the colliding NO + Ar pair will produce the perturbing interaction to destroy the NO coherent oscillations initially prepared by the combined Stark and RF field. In other words, only those NO + Ar configurations whose interaction energies could couple with the 12.2 kHz coherent oscillation will result in a loss of coherence.

The NO + Ar long-range interaction potential can be described by the dipole−induced dipole model potential given by[17]

$$V_{int} = -\frac{\mu_{NO}^2\cdot\alpha_{Ar}}{R^6} \quad (16)$$

where μ_{NO}, α_{Ar}, and R stand for the NO permanent dipole moment, the Argon atomic polarizability, and the interparticle distance, respectively. Using the literature values for $\mu_{NO} = 0.158$ D[20−22] and $\alpha_{Ar} = 1.63$ Å,[23] eq 16 predicts that a NO molecule will "feel" an interaction potential of 12.2 kHz when the Ar approaches exactly at a distance of $R_d = 28.03$ Å^2.

This critical value gives an effective decoherence cross-section $\sigma_d = \pi R_d^2 = 2.47 \times 10^3$ Å^2, which lies within 5% with respect to the experimentally deduced value of 2.58×10^3 Å^2 .These results explain why the decoherence cross-section has a significantly different value and, what is more important, reveals the specific dynamics underlying, in the present case, the collisional decoherence. When the colliding particles experience an interaction potential whose energy value is resonant with energy of the coherent oscillation, the coupling between the "internal" motion and the "external" perturbation destroys the prepared coherent state.

It is interesting to note the high sensitivity of the employed methodology to prepare and destroy coherent states using RF fields. Since the rephasing of the molecular beam can be achieved using a wide range of RF frequencies and distinct polar molecules, the present experimental technique provides a highly sensitive probe of the interaction potential as a function of the interparticle distance.

The proposed dynamical model to describe the collision decoherence provides a direct connection between the observed oscillatory frequency spacing $\Delta\nu_{osc}$ and the two-particle interaction potential. Indeed, these quantities can be related by eq 17:

$$h\Delta\nu_{osc} = |V_{int}(R = R_d)| = \frac{\pi^3\mu_m^2\alpha_g}{\sigma_d^3} \quad (17)$$

where h is Planck's constant, $\sigma_d = \pi R_d^2$ is the effective decoherence cross-section, μ_m is the electric dipole moment of the molecule forming the beam, and α_g is the atomic polarizability of the scattering partner. In summary, the experimental observables $\Delta\nu_{osc}$ and σ_d allow us to deduce the value of μ_m if α_g is known or the other way around.

SUMMARY AND CONCLUSIONS

The present work represents a step forward in the systematic study of the interaction between a polar beam and static and RF electric fields, a subject that constitutes the research activity of our group since recent years. Here, the emphasis is on the

dx.doi.org/10.1021/jp401005v | J. Phys. Chem. A 2013, 117, 8119−8125

measurement of the quantum decoherence by induced (single) collision experiments between the initially prepared coherent beam and a rare gas partner.

The first conclusion we would like to draw from the reported work and results concerns the novelty and simplicity of the method. The basic ingredients that this new experimental setup requires are a beam of polar molecules and a secondary chamber where (i) the coherent superposition of the internal states of the molecule under study (the first partner) is produced and (ii) the collisional experiment is implemented by adding, in a controlled manner, the second collisional partner, the scattering gas (Ar in the present case).

It is remarkable to point out that these ingredients constitute the basic know-how of the traditional molecular beam technology with the inclusion of a simple RF unit, a device that belongs to the well-known molecular beam electric resonance methodology.

Besides the previous consideration, one of the most important conclusions we would like to point out is the capability of the technique to measure the decoherence cross-section and the subsequent finding of the great difference (ca. 1 order of magnitude) between the measured total attenuation cross-section and the total decoherence cross-section for NO + Ar collisions at an average relative velocity of $\overline{v}_R \sim 1.3.10^3 m{\cdot}s^{-1}$.

To rationalize the significant difference between both cross-section values, a collision model was introduced based on the NO + Ar dipole−induced dipole potential. Essentially, the basic features underlying the distinct dynamics responsible for the very different cross-section values involve the contribution of rather different trajectories for each process.

It was argued that, while there are NO + Ar trajectories whose scattering angle is confined within the NO beam divergence and, therefore, make no contribution to the total attenuation cross-section, they, nevertheless, may destroy the coherent superposition and, consequently, contribute to the total decoherence cross-section. With respect to this quantity, the satisfactory agreement between the value predicted by the model and that deduced from the experimental data was remarkable.

Despite the obtained quantitative agreement, it should be remarked that the theoretical model developed is a simple one aimed at rationalizing the observed data for the NO + Ar decoherence cross-section. There was no intention to present it as a general treatment. For such a claim, one would have to wait until new results become available for other collision systems. This work will be carried out in our laboratory including the investigation of quantum decoherence in reactive collisions.

AUTHOR INFORMATION

Corresponding Author

*E-mail: laseres@pluri.ucm.es Telephone: ++34913943260.

Author Contributions

▽These authors contributed equally.

Notes

Part of this work was presented in the Rarefied Gas Dynamic Conference (RGD 28) held in Zaragoza (Spain) July, 2012.
The authors declare no competing financial interest.

ACKNOWLEDGMENTS

Financial support from the Ministerio de Educación y Ciencia of Spain (Grants CTQ2007-61749 and CSD2009-00038) is gratefully acknowledged

REFERENCES

(1) Nielsen, M. A.; Chuang, I. L. *Quantum Computation and Quantum Information*, 10th Anniversary ed.; Cambridge University Press: New York, 2010.

(2) Miffre, A.; Jacquey, M.; Büchner, M.; Trénec, G.; Vigué. Atom interferometry. *J. Phys. Scr.* **2006**, *74*, C15−C23.

(3) Shapiro, M.; Brumer, B. *Principles of the Quantum Control of Molecular Processes*; John Wiley & Sons Publication: Hoboken, NJ, 2003.

(4) Rice, S. A.; Zhao, M. *Optical Control of Molecular Dynamics*; John Wiley & Sons: New York, 2000.

(5) Orr-Ewing, A. J.; Zare., R. N. Orientation and Alignment of Reaction Products. *Annu. Rev. Phys. Chem.* **1994**, *45*, 315−366.

(6) Wheeler, J. A.; Zurek, V. H. *Quantum Theory of Measurements*: Princeton University Press: Princeton, NJ, 1983.

(7) See, for example, Schlosshauer, M. Decoherence, the Measurement Problem, and Interpretations of Quantum Mechanics. *Rev. of Mod. Phys.* **2005**, *76*, 1267−1305.

(8) Brune, M.; Hagley, E.; Dreyer, J.; Maitree, X.; Maali, A.; Wunderlich, C.; Raimon, J. M.; Haroche, S. Observing the Progressive Decoherence of the "Meter" in a Quantum Measurement. *Phys. Rev. Lett.* **1996**, *77*, 4887−4890.

(9) Takahashi, S.; Tupitsyn, I. S.; van Tol, C. C.; Beedle, J.; Hendrickson, D. N.; Stamps, P. C. E. Decoherence in Quantum Magnets. *Nature* **2001**, *476*, 76−79.

(10) Hornberger, K.; Uttenhaler, S.; Brezger, B.; Hackermüller, L.; Arndt, M.; Zeilinger, A. Collisional Decoherence Observed in Matter Wave Interferometry. *Phys. Rev. Lett.* **2003**, *90*, 160401.

(11) Penrose, R. On Gravity's Role in Quantum State Reduction. *Gen. Relativ. Gravitation* **1996**, *28*, 581−600.

(12) Tegmark, M. Apparent Wave Function Collapse Caused by Scattering. *Found. Phys. Lett.* **1993**, *6*, 571−590.

(13) Gallis, M. R.; Fleming, G. N. Environmental and Spontaneous Localization. *Phys. Rev.* **1990**, *A 42*, 38−48.

(14) Brezger, B.; Hackermüller, L.; Uttenthaler, S.; Petschinka, J.; Arndt, M.; Zeilinger, A. Matter-Wave Interferometer for Large Molecules. *Phys. Rev. Lett.* **2002**, *88*, 100404.

(15) Gasmi, K.; Gonzálvez, A. G.; González Ureña, A. Interferences in the Transverse Profile of a Toluene Beam Induced by a Resonant RF Electric Field. *J. Phys. Chem. A* **2010**, *A 114*, 3229−3236.

(16) Dagdigian, P. J.; Cruse, H. W.; Zare, R. N. Laser Fluorescence Study of AlO Formed in the Reaction Al + O_2: Product State Distribution, Dissociation Energy, and Radiative Lifetime. *J. Chem. Phys.* **1975**, *62*, 1824−1833.

(17) Levine, R. D.; Bernstein, R. B. *Molecular Reactions Dynamics*; Oxford University Press: Oxford, U.K., 1974. See Chapter 2.

(18) Thuis, H. H. W.; Stolte, S.; Reuss, J.; van der Biesen, J. J. H.; van der Meijdenberb, C. C. H. Angle Dependent Interaction Potentials for NO+Ar, NO+Kr and NO+Xe Derived From Various Total Collision Cross Section Data. *Chem. Phys.* **1980**, *52*, 211−225.

(19) Thuis, H. H. W.; Stolte, S.; Reuss, J. Investigation of the Angle Dependent Part of the Intermolecular Potential of NO−inert Gas Systems Using Crossed Molecular Beams. *Chem. Phys.* **1979**, *43*, 351−364.

(20) Neumann, R. M. High-Precision Radiofrequency Spectrum of $^{14}N^{16}O$. *Astrophys. J.* **1970**, *161*, 779−784.

(21) Gijsbertsen, A.; Siu, W.; Kling, M. F.; Johnsson, P.; Jansen, P.; Stolte, S.; Vrakking, M. J. J. Direct Determination of the Sign of the NO Dipole Moment. *Phys. Rev. Lett.* **2007**, *99*, 213003.

(22) Cáceres, J. O.; Montero, C.; Morato, M.; Gonzalez Ureña, A. Interaction of a Supersonic NO Beam with a Static and a Resonant RF Field: Measurement of Rotationally Resolved Dipole Moments. *Chem. Phys. Lett.* **2006**, *426*, 214−218.

(23) *Handbook of Chemistry and Physics*, 90th ed.; Lide, D. R., Ed.; Taylor & Francis: Boca Raton, FL, 2009.